

# Refined Astrometry and Positions for 179 Swift X-ray Afterglows

N. R. Butler<sup>1,2</sup>

## ABSTRACT

We present a refined catalog for the positions of 179  $\gamma$ -ray burst (GRB) X-ray afterglows observed by the X-ray Telescope (XRT) on Swift prior to November 1, 2006. The positions are determined by detecting X-ray field sources in the deep X-ray images and comparing the centroids to those of optical sources in the Digitized Sky Survey (DSS) red2 catalog or the Sloan Digital Sky Survey (SDSS) DR-5 catalog. Half of the 90% confidence error region radii are  $< 2.2$  arcseconds. The error regions areas are typically  $\sim 4$  times smaller than the best XRT-team error regions, although the positions require deep X-ray integration ( $> 20$  ksec) and cannot be generated nearly as rapidly after the GRB. The positions derived for  $> 90\%$  of 77 bursts with optical afterglows are consistent with the optical transient positions, without the need for systematic error. About 20% of the afterglows positions require a sizable shift in the Swift satellite aspect. We discuss the optical/X-ray properties of the field sources and discuss implications of the frame offsets for studies of optically dark GRBs.

*Subject headings:* gamma rays: bursts — supernovae: general — X-rays: general — telescopes

## 1. Introduction

The *Swift* satellite (Gehrels et al. 2004) is revolutionizing our understanding of  $\gamma$ -ray bursts and their afterglow emission. Key to *Swift's* success are the rapid localization capability and unprecedented detection sensitivity of the Burst Alert Telescope (BAT; Barthelmy et al. 2005) and the capability of the X-ray Telescope (XRT; Burrows et al. 2005) to determine  $\sim 5''$  positions for the burst afterglows within minutes of the BAT  $\sim 3'$  source localizations. These localizations have enabled the detection and study of  $\sim 80$  GRB optical afterglows since the satellite launch in late 2004 and prior to November 1, 2006.

---

<sup>1</sup>Townes Fellow, Space Sciences Laboratory, University of California, Berkeley, CA, 94720-7450

<sup>2</sup>Astronomy Department, University of California, 445 Campbell Hall, Berkeley, CA 94720-3411, USA

The pointing direction of the *Swift* satellite is determined by star trackers with an accuracy  $\lesssim 5''$ . However, X-ray sources are typically centroided much more finely ( $\lesssim 1''$ ), and the GRB afterglow position errors quoted by the XRT team are dominated by systematic error terms which account for the poor relative accuracy of the star trackers. Recently, Moretti et al. (2006) have refined the XRT boresight calibration (which relates the XRT alignment to the star tracker positions) and effectively reduced the systematic position error by a factor of two for 68 afterglows. Here, we present a methodology for sidestepping the satellite instrument alignment and pointing uncertainties which decreases the position errors by an additional factor of two. We present refined X-ray positions for 179 bursts determined by matching X-ray field source positions directly to those of counterpart optical sources. The sample of 179 bursts is that for which the XRT team has published positions in the  $\gamma$ -ray Coordinates Network (GCN) circulars and in Moretti et al. (2006).

## 2. X-ray Source Detection and Centroiding

The *Swift* XRT Position Counts (PC) mode data are reduced by running the `xrtpipeline` reduction task from the HEASoft 6.0.6<sup>3</sup> software release and using calibration files from the most recent calibration database release (2006-04-27). Starting with a position guess for the afterglow, we map the counts from each followup observation onto a tangent plane centered at that position. Detections of and positions for X-ray field sources in the composite image with signal-to-noise ratio  $> 3$  are found by running `wavdetect` (Freeman et al. 2002) on scales  $2, 2\sqrt{2}, 4, 4\sqrt{2},$  and  $8$  pixels. To additionally reject spurious sources, we require the `wavdetect` sources to have an estimated size  $> 5$  pixels and to have aspect ratios  $< 2$ . We also reject highly variable X-ray (KS-test prob.  $< 10^{-10}$ ) sources, which are typically spurious sources or sources off-chip for a portion of the observation.

Special attention is paid to the centroiding of the afterglow, which is taken to be the most significant and variable source within a  $50 \times 50$  pixel<sup>2</sup> region about the position guess. The XRT team positions are used for the position guess. In the few cases where the afterglow faintness leads to more than one possible candidate, we adopt the candidate selected by the XRT team. A maximum likelihood (ML) centroiding algorithm is used for the XRT PC mode counts extracted in a  $20 \times 20$  pixel<sup>2</sup> region about this source.

The likelihood for the observed counts  $i$  (positions  $x_i, y_i$  and energy  $E_i$ ) as a function

---

<sup>3</sup><http://heasarc.gsfc.nasa.gov/docs/software/lheasoft/>

of the source position  $(x_o, y_o)$  can be written:

$$\mathcal{L} = C^N \left\{ \prod_{i=1}^N \Phi_{\text{psf}}(x_i - x_o, y_i - y_o, E_i) \right\} \exp \left\{ -C \iint dx dy \Phi_{\text{psf}}(x - x_o, y - y_o) M(x, y) \right\}, \quad (1)$$

where  $C$  is a normalization,  $M$  is a (source-flux-weighted) exposure map, and  $\Phi_{\text{psf}}$  is the point spread function model from the calibration database (`swxpsf20010101v003.fits`). The term in the exponential rigorously accounts for the presence of bad or missing detector columns or pixels. We maximize this expression with respect to  $C$ , and use the following fit statistic for  $N$  total counts for the centroiding:

$$\chi^2 = 2N \log \left\{ \iint dx dy \Phi_{\text{psf}}(x - x_o, y - y_o) M(x, y) \right\} - 2 \sum_i \log[\Phi_{\text{psf}}(x_i - x_o, y_i - y_o, E_i)]. \quad (2)$$

Circular error regions are determined by numerical integration for each centroid.

The calculated position error at 90% confidence versus the number of detected source counts  $C$  for 179 burst afterglows is well described as a powerlaw  $13.4 C^{-1/2}$  arcsec, with significant scatter below 20 counts. Comparing the centroids for the bursts with optical transient (OT) positions, we find that the ML centroids are on average 10% more accurate than centroids determined using the `xrtcentroid` task. The empirical errors from that tool and XRT data have been found to follow  $23 C^{-0.48}$  (Hill et al. 2005; Moretti et al. 2006), which is typically a factor  $\sim 2$  larger than for the ML centroider.

### 3. Probabilistic X-ray Image Registration to Optical Catalogs

We begin with a deep X-ray exposure and the comparison of the X-ray source positions to the positions of optical sources. If data from the Sloan Digital Sky Survey (SDSS; Adelman-McCarthy et al. 2006) are present for a given X-ray afterglow field, we download the catalog data and fits images. We also download the Digitized Sky Survey (DSS2-red) images and the USNO-B2 catalog for the field. We then run `sextractor` (Bertin & Arnouts 1996) over the images to generate the deepest possible catalog ( $r' \lesssim 22.5$  for SDSS,  $R \lesssim 20$  for DSS). The DSS astrometry is corrected to sub-arcsecond levels using the Two Micron All Sky Survey.

For each `wavdetect` X-ray source  $i$ , we record the positions of optical sources  $j$  within a box of area  $A$  equal to  $20 \times 20$  arcsec<sup>2</sup>. We consider each optical source an equally likely possible counterpart to X-ray source  $i$ . The probability distribution for the offset of the

X-ray image from the optical image, given this one source, can be written:

$$P_{X,i} = \frac{P_0}{A} + (1 - P_0) \sum_j G([x_j - x_i]^2 + [y_j - y_i]^2, \sigma_i), \quad (3)$$

where the sum of Gaussian terms  $G$  is normalized over the allowed area  $A$ . Here, the positions  $x$  and  $y$  are related to shifts in right ascension  $\Delta\alpha$  and declination  $\Delta\delta$  approximately by  $x = \Delta\alpha \cos(\delta)$  and  $y = \Delta\delta$ , both in arcseconds. The prior-probability of finding an optical/X-ray match is  $P_0$ . Based on fields searched prior to 2006 (see also Section 4.2 below), we set these to be 1/2 and 1/3 for the SDSS and DSS, respectively. We allow for the possibility of a small frame rotation by replacing each term  $G$  in equation (3) with

$$\bar{G} = \frac{1}{\sqrt{2\pi\sigma_\theta^2}} \int d\theta G([x_j - x_i - \theta(y_i - y_p)]^2, [y_j - y_i + \theta(x_i - x_p)]^2, \sigma_i) \exp\left\{-\frac{\theta^2}{2\sigma_\theta^2}\right\}, \quad (4)$$

where  $(x_p, y_p)$  is the XRT aim point. In marginalizing over the unknown rotation angle, we assume a Gaussian prior with  $\sigma_\theta = 5'$ . Combining the information from each X-ray field source, the offset probability can be written:

$$P_{X-\text{opt}} = \frac{1}{2\pi\sigma_r^2} \exp\left\{-\frac{x^2 + y^2}{2\sigma_r^2}\right\} \prod_i P_{X,i}, \quad (5)$$

where we use a Gaussian prior that the offset radius is  $0 \pm \sigma_r$ , with  $\sigma_r = 3''$ . Figure 1 shows example Optical—X-ray positions and probabilities derived for the GRB 050408 and GRB 060108 fields. In the backgrounds, we plot  $-2\log(P_{X-\text{opt}})$ .

As we discuss below, a relatively long total exposure ( $> 20$  ksec) over several orbits is required to detect and match X-ray field sources. Because the satellite re-acquires the field every orbit, we expect (and observe) there to be a scatter in the aspect solution for different visibility periods. It is therefore possible that the position offset for the period of bright GRB afterglow activity is not the same as the mean frame offset determined from the full integration.

To account for the effect of shifting aspect during the observations of an afterglow over several days or weeks, we co-add the counts in  $20 \times 20$  pixel<sup>2</sup> regions about each X-ray field source. An additional composite field star image is formed by replacing the total field star counts in each good time interval of data acquisition by the counts detected for the afterglow in that interval. We then determine the afterglow offset relative to the mean frame offset by spatially shifting the counts-weighted composite field star image until it overlaps with the first composite field star image. This calculation typically contributes error  $\sim 1$  arcsec, although this can be considerably larger for faint or rapidly fading sources.

## 4. Discussion

### 4.1. Comparison With Optical Transient and XRT Team Positions

Tables 1–3 give our X-ray positions for 179 *Swift* GRB afterglows with X-ray positions quoted in the GCN. In most cases, we cleanly detect the X-ray transient and observe it to fade in time. In a few cases (GRB 050906 GCN3956, GRB 050911 GCN3967, GRB 050925 GCN4043, GRB 060223B GCN4835) the fades are only weakly confirmed, consonant with the XRT Team’s reports that these sources are only candidates. These positions should be treated with caution. Figure 2 shows the best-fit offset calculated for each of the 179 afterglows. Ninety percent of the offsets are  $\lesssim 4''$ . The scatter is similar to the systematic error ( $3.2''$ , 90% conf.) introduced in Moretti et al. (2006). Both the position offsets relative to the known OT positions (Figure 3) and the reported errors (Figure 3A) decrease by 50% on average, relative to those reported by the XRT team. We find that  $\gtrsim 90\%$  of the 77 source positions lie within our computed error (statistical only) of the OT positions, also accounting for the error in the OT positions. A large fraction  $\sim 90\%$  of the XRT Team positions are also consistent with the OT positions. Finally, we note that  $40/179 = 22\%$  of our positions lie beyond the quoted XRT error radius from the XRT team position. The positions for these bursts are underlined in Tables 1–3. If we restrict to just the bursts with refined positions quoted in Moretti et al. (2006), 13% of the positions are discrepant.

### 4.2. Properties of the Optical/X-ray Field Sources

In this and the next section, we consider *Swift* bursts detected prior to September 11, 2006, corresponding to the date of submission of this paper. For this time period, 49% (35%) of the X-ray field sources have optical sources in the SDSS (DSS) within  $2''$ . This justifies our choice of priors on the match probability (Section 3). The choice of priors leads to tighter error bars from an SDSS catalog match than for the DSS catalog match.

From deep field observation with *Chandra* (Giacconi et al. 2001),  $\approx 90\%$  of X-ray sources brighter than  $F_X \approx 3 \times 10^{-16}$  erg cm $^{-2}$  s $^{-1}$  have optical counterparts brighter than  $R = 26$ . The *Chandra* source counts at higher flux levels (Figure 7 Giacconi et al. 2001) appear consistent with the detection fraction quoted above, where  $F_X > 2 \times 10^{-15}$  erg cm $^{-2}$  s $^{-1}$  and  $R < 20$  (DSS) or  $r' \lesssim 22.5$  (SDSS). There is considerable scatter about the  $F_X/F_{\text{opt}} = 1$  line (solid line in Figure 4), which describes *ROSAT* sources in the Lockman Hole (Hasinger et al. 1998). We observe a weak  $\tau_{\text{Kendall}} = -0.09$  (although  $5\sigma$  significant) correlation of the optical  $R$ -band magnitude with X-ray flux. There is a large scatter  $\sim 1.7$  mag, roughly independent of the X-ray flux. Here, we ignore the difference between the  $r'$  and  $R$  bands, and we adopt

a constant scaling of  $5 \times 10^{-11}$  erg cm<sup>-2</sup> rate<sup>-1</sup> in order to convert the observed XRT rate in counts per second to flux.

### 4.3. Implications for Optically Dark Bursts and GRB Host Galaxies

Our refined positions for 39 of 160 X-ray afterglows lie outside of the error regions determined by the XRT team. This fraction is one possible metric on the fraction of potential missed optical source associations— either afterglows or host galaxies—because even modest shifts in the refined positions relative to those quoted by the XRT team can allow previously excluded regions of sky and can have important consequences for the optical source associations (see, e.g., Bloom et al. 2006).

The fraction of missed afterglows must be smaller than 39/160, because bright afterglows should be detected independent of modest X-ray positions misdeterminations. An OT is most likely to be detected either when the position lies inside the XRT team error region or when the OT is sufficiently bright. As a proxy for the fraction of bright OTs, we take the fraction of the 39 bursts with poor positional agreement, for which an OT was nonetheless detected ( $P_{\text{bright}} = 14/39$ ). Faint afterglows would have been detected for only the bursts with excellent positional agreement ( $P_{\text{good pos}} = 121/160$ ). We should then find that  $P_{\text{bright}} + P_{\text{faint}} P_{\text{good pos}} = 69/160$ , the observed OT detection fraction. The bursts are either optically bright, faint, or dark. From this, we calculate the fraction of optically faint bursts  $P_{\text{faint}} \approx 9\%$ , implying that only  $\approx 4$  OTs may have been missed in the sample of 39 X-ray afterglows with position offsets. One well-documented example of such a case is GRB 060108 for which our SDSS-refined X-ray position (Butler & Bloom 2006) led to the detection of the infra-red afterglow (Oates et al. 2006), located just outside the XRT-team refined error region.

Although we conclude that future refined positions are unlikely to dramatically increase the number of OTs detected, we do plan to make the positions available to the community as rapidly as possible. X-ray field source detection apparently works well for afterglows observed for  $\Delta t \gtrsim 20$  ksec, with the tightest possible error regions becoming possible for  $\Delta t \gtrsim 50$  ksec. These exposures have typically occurred within 1 to several days after a bursts. Our positions are autonomously determined on these timescales and are published on the web<sup>4</sup>. Because the position and error radius change in time as more data are accumulated, consumers should quote the version number (incremented from the version 0.0 positions quoted here) when referencing one of these positions.

---

<sup>4</sup>[http://astro.berkeley.edu/~nat/swift/xrt\\_pos.html](http://astro.berkeley.edu/~nat/swift/xrt_pos.html)

The refined positions may be most useful for host galaxy studies. For example, there is evidence for an over-density of bright optical sources within our error regions. The optical/X-ray match fractions translate to an average optical source density of  $(1.55 \pm 0.03) \times 10^{-3}$  arcsec $^{-2}$  ( $R \lesssim 20$ ) and  $(2.74 \pm 0.09) \times 10^{-3}$  arcsec $^{-2}$  ( $r' \lesssim 22.5$ ). There are enough (120) DSS images with error radii  $< 5''$  to allow for the determination of the density within the error region: 8 sources or a density of  $(4 \pm 1) \times 10^{-3}$  arcsec $^{-2}$  (Figure 5). We conclude from this significant over-density that most of these sources—aside from one associated with GRB 050721 which occurred at Galactic latitude  $|b| < 10$ —may be bright GRB host galaxies. Consonant with an interpretation that these events are relatively nearby,  $\sim 3$  are X-ray Flashes. We note that none are short/hard GRBs. The only burst with a measured redshift is GRB/XRF 060218 ( $z = 0.0331$ ; Mirabal et al. 2006). The SDSS image shows a spatially extended host galaxy (Mirabal 2006). Several of the other possible host galaxies in Figure 5 appear to possibly be extended. The only other source in the list of 8 which has a detected OT is GRB/XRF 060428B. Perley et al. (2006b) have explored the possibility that this nearby ( $z = 0.348$ ) galaxy may physically associated and conclude that it is not. Finally, although the core of the potential host galaxy is not in our error region, Perley et al. (2006a) report that our position for GRB 051109B lies in the spiral arm of a bright galaxy (Figure 5).

## 5. Conclusions

We present a catalog of 179 positions for the X-ray afterglows of *Swift* GRBs, with astrometry solutions determined by matching optical positions to those of X-ray field sources. On average, the position are determined with a factor of two more accuracy and with 50% smaller error radius estimates than when the astrometry correction is neglected and the satellite aspect solution is assumed. The typical position error is  $2.2''$ , with no systematic error term. There is now very little chance ( $< 2\%$ ) of source confusion in the XRT error regions. The properties of the optical/X-ray field sources observed in 1.9 Msec of PC mode data appear to be similar to sources observed (in the bright end) in deep field surveys. There is an indication of bright host galaxies in our error regions of nine afterglows. We hope that our positions will facilitate deep observations of potential host galaxies for a large fraction of past and future GRBs with *Swift* XRT afterglows.

N. Butler gratefully acknowledges support from a Townes Fellowship at the U. C. Berkeley Space Sciences Laboratory, as well as partial support from J. Bloom and A. Filippenko. Special thanks to J. Bloom for many useful discussions. We thank an anonymous referee for useful and insightful criticism.

## REFERENCES

- Adelman-McCarthy, J. K., et al. 2006, *ApJS*, 162, 38
- Barthelmy, S. D., et al. 2005, *Sp. Sc. Rev.* in press, astro-ph/0507410
- Bertin, E., & Arnouts, S. 1996, *A&AS*, 117, 393
- Burrows, D. N., et al. 2005, *Sp. Sc. Rev.* in press, astro-ph/0508071
- Butler, N. R., & Bloom, J. S. 2006, GCN #4500
- Bloom, J. S., et al. 2006, *ApJAccepted*, astro-ph/0607223
- Freeman, P. E., et al. 2002, *ApJS*, 138, 185
- Gehrels, N., et al. 2004, *ApJ*, 611, 1005
- Giacconi, R., et al. 2001, *ApJ*, 551, 624
- Hasinger, G., et al. 1998, *A&A*, 329, 482
- Hill, J. E. et al. 2005, *Proc. SPIE*, 5898, 313
- Mirabal, N. 2006, GCN #4783
- Mirabal, N., et al. 2006, GCN #4792
- Moretti, A., et al. 2006, *A&A*, 448, L9
- Oates, S. R., et al. 2006, *MNRAS* accepted, astro-ph/0607601
- Perley, D., et al. 2006a, GCN #5387
- Perley, D., et al. 2006b, in prep.



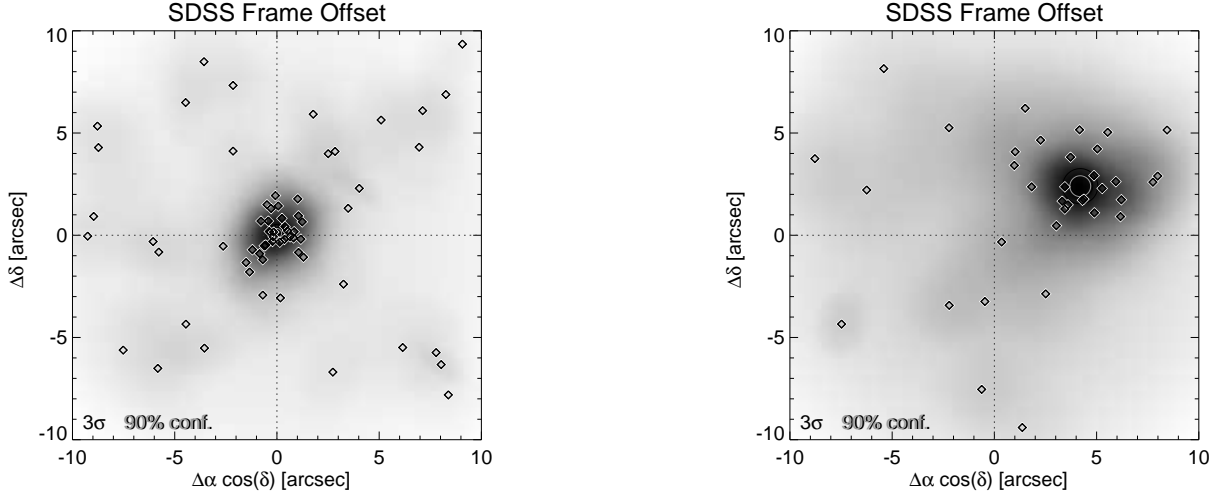


Fig. 1.— Example frame offset probability plots for GRB 050408 and GRB 060108. The points are the SDSS optical source positions relative to the X-ray source positions. The shaded background describes the offset probability between the optical and X-ray field sources (Section 3). For GRB 050408, the best fit frame offset is  $\Delta\alpha = 0.0$ ,  $\Delta\delta = -0.1$ ,  $\pm 0.3$  [arcsec] 90% Conf. For GRB 060108 (Butler & Bloom 2006; Oates et al. 2006), the best fit frame offset is  $\Delta\alpha = 4.2$ ,  $\Delta\delta = 2.4$ ,  $\pm 0.5$  [arcsec] 90% Conf. We also plot 90% confidence and  $3\sigma$  error circles.

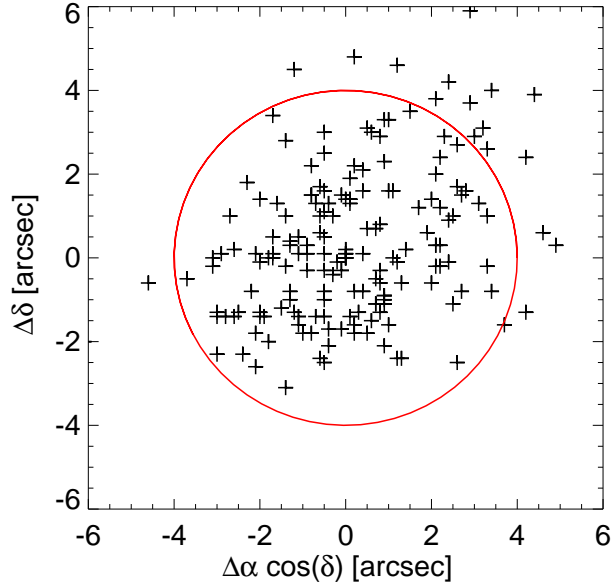


Fig. 2.— XRT Frame Offsets for 179 Bursts relative to DSS/SDSS. 90% of the offsets are contained within the red,  $4''$  radius circle. This radius is comparable to the XRT team systematic error.

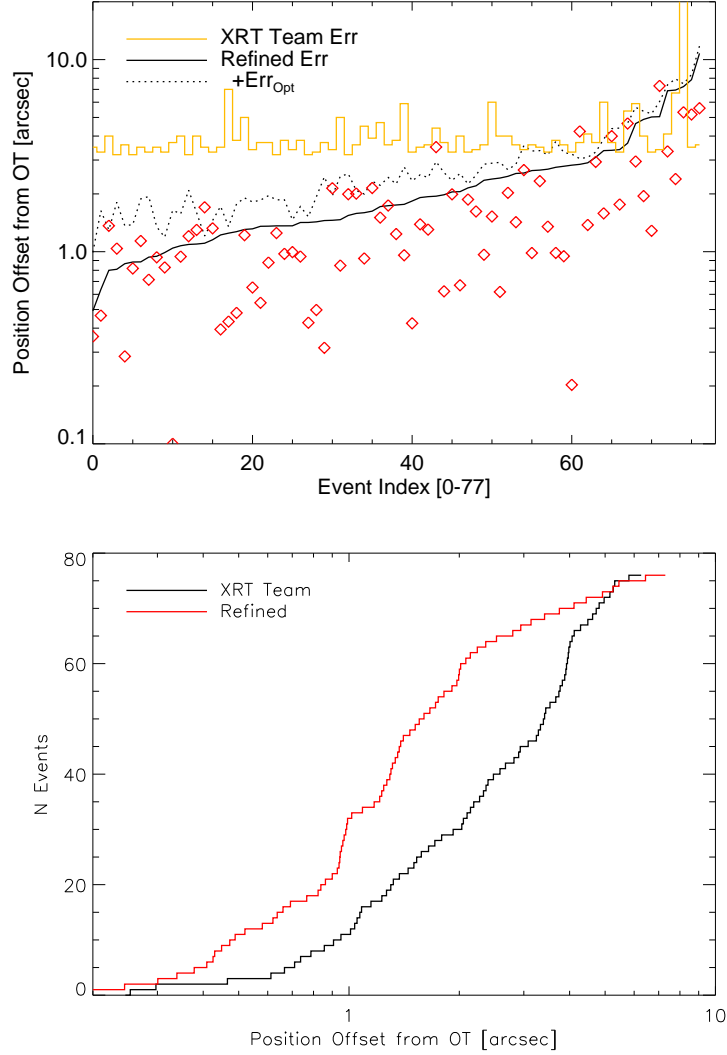


Fig. 3.— (A) Comparison of the final X-ray position differences from the optical transient positions in the literature (red points). The X-ray position 90% confidence error is overplotted (solid black curve), as is the X-ray plus OT position error (dotted curve). The median offset is 1.3 arcsec. The median error (X-ray only) is 1.8 arcsec. Of the X-ray positions,  $71/77 = 92\%$  are consistent with the optical positions. The orange (histogram) curve shows the XRT team error radius for each event. The offset of the XRT team positions from the OT positions are not plotted. However, we note that  $68/77 = 88\%$  of the XRT team positions are consistent with the OT positions. (B) Cumulative plot of the positions offsets relative to the OT positions for the refined and XRT team positions. The nearly constant logarithmic shift over a range of offsets corresponds to a factor of two increase in positional accuracy. From a KS-test, the probability that the two offset distributions are drawn from the same distribution is  $10^{-5}$ .

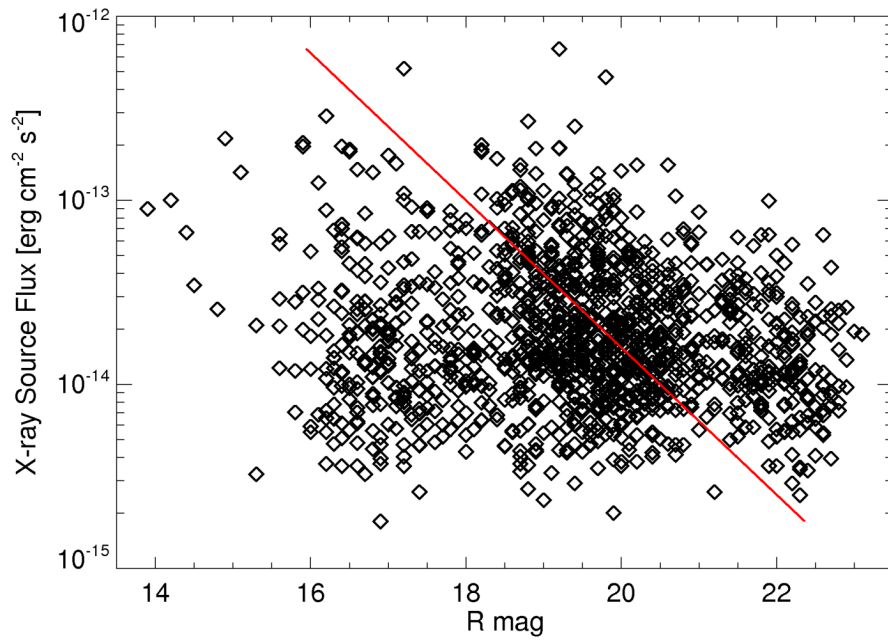


Fig. 4.— The X-ray fluxes and optical magnitudes for matched sources between the XRT and DSS/SDSS. Missing from the plot are the non-detections ( $R > 22$ ) for  $\sim 1/3$  of the X-ray sources. The solid red line shows the best fit curve from deep field observations with *ROSAT* and *Chandra* (Hasinger et al. 1998; Giacconi et al. 2001). There is considerable scatter about that line.

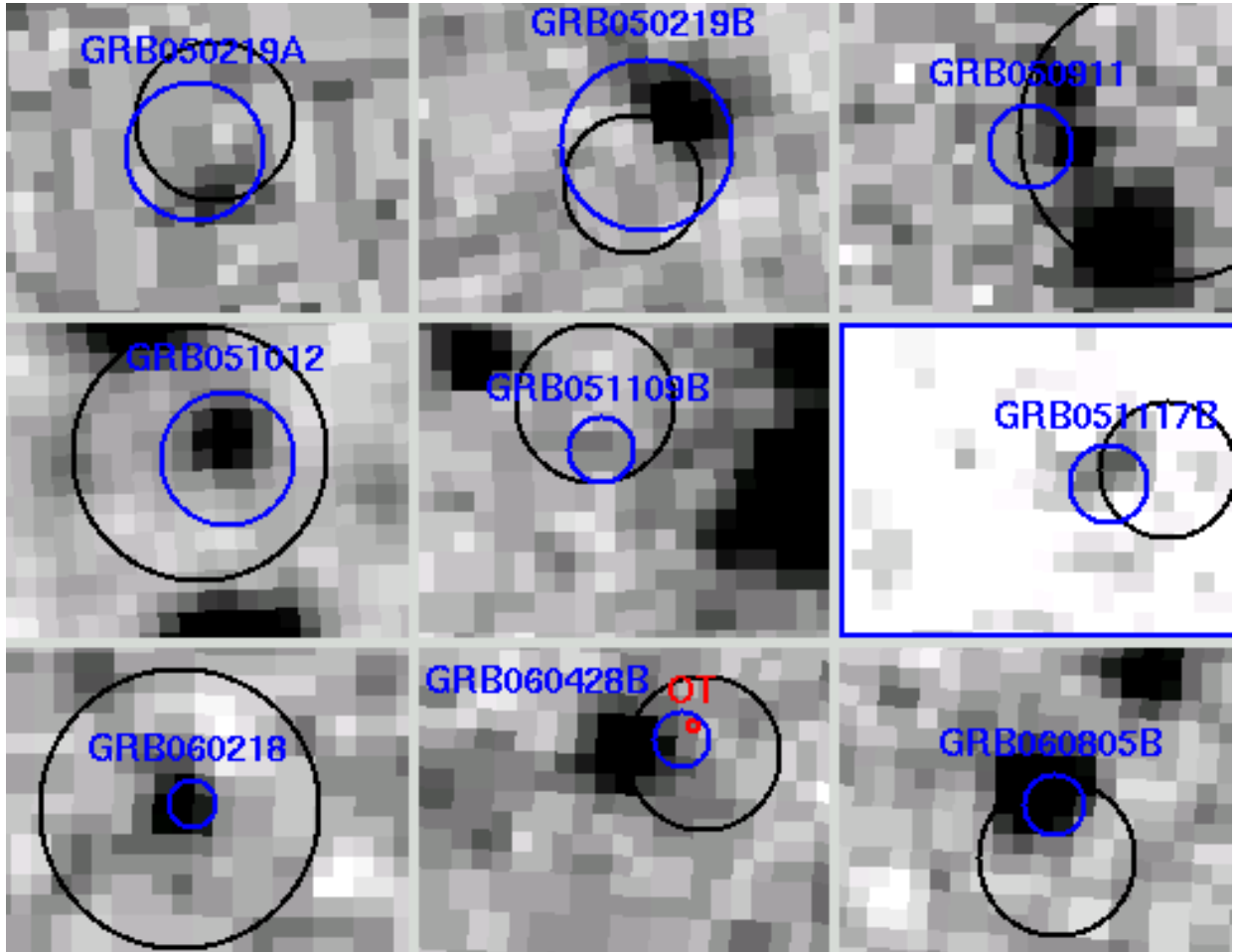


Fig. 5.— DSS images of nine refined X-ray positions regions (circles) which are consistent with bright optical sources. Aside from the bright spiral galaxy to the West of GRB 051109B (with  $R \sim 14.5$ ), the optical magnitudes range from  $R = 18.3 - 20.5$ . Our error regions are shown in blue, with the XRT team error circles in black. In most cases (but not all) the refined error regions are smaller. In all cases, the refined error regions better identify the optical association.

Table 1: Astrometrically-corrected XRT GRB Afterglow Positions

GRB	$\alpha$ (J2000)	$\delta$ (J2000)	Err <sub>90</sub> ["]	GRB	$\alpha$ (J2000)	$\delta$ (J2000)	Err <sub>90</sub> ["]
050408 <sub>16</sub>	12 02 17.36	+10 51 10.5	1.2 <sup>a</sup>	050505 <sub>4</sub>	09 27 03.34	+30 16 24.6	0.8 <sup>a</sup>
050504	13 24 01.18	+40 42 14.3	4.6 <sup>a</sup>	050509A	20 42 19.88	+54 04 19.4	2.5 <sup>b</sup>
050520	<u>12 50 05.94</u>	<u>+30 27 03.2</u>	2.4 <sup>a</sup>	050509B	12 36 14.06	+28 59 07.2	3.4 <sup>a</sup>
050522	13 20 34.57	+24 47 20.7	3.8 <sup>a</sup>	050525 <sub>48</sub>	18 32 32.67	+26 20 21.2	2.1 <sup>b</sup>
050714A	02 54 23.33	+69 06 45.1	2.7 <sup>b</sup>	050528	<u>23 34 04.35</u>	<u>+45 58 21.8</u>	2.9 <sup>b</sup>
051012	18 02 10.95	-52 47 12.6	3.4 <sup>b</sup>	050603 <sub>7</sub>	02 39 56.90	-25 10 55.7	0.9 <sup>b</sup>
051021A <sub>47</sub>	01 56 36.41	+09 04 04.3	2.1 <sup>b</sup>	050607 <sub>29</sub>	20 00 42.77	+09 08 31.1	1.4 <sup>b</sup>
051022 <sub>12</sub>	23 56 04.08	+19 36 23.3	1.1 <sup>b</sup>	050701	15 09 01.67	-59 24 55.6	2.4 <sup>b</sup>
051028 <sub>59</sub>	<u>01 48 14.97</u>	<u>+47 45 08.3</u>	2.8 <sup>b</sup>	050712	05 10 48.34	+64 54 46.9	1.4 <sup>b</sup>
051105B	00 37 53.73	-40 29 16.3	2.8 <sup>b</sup>	050713A <sub>61</sub>	21 22 09.54	+77 04 29.7	2.8 <sup>b</sup>
051211B <sub>35</sub>	23 02 41.50	+55 04 50.8	1.6 <sup>b</sup>	050713B	20 31 15.59	+60 56 41.9	1.0 <sup>b</sup>
060121 <sub>22</sub>	09 09 52.00	+45 39 45.4	1.4 <sup>a</sup>	050714B	11 18 47.75	-15 32 49.3	2.1 <sup>b</sup>
060123	11 58 47.83	+45 30 50.9	1.0 <sup>a</sup>	050716	22 34 20.72	+38 41 03.6	0.9 <sup>b</sup>
060805B	18 10 05.57	+58 09 18.9	1.5 <sup>b</sup>	050717	14 17 24.61	-50 31 59.9	3.6 <sup>b</sup>
060901	19 08 38.02	-06 38 09.0	6.7 <sup>b</sup>	050721 <sub>67</sub>	16 53 44.40	-28 22 52.2	3.4 <sup>b</sup>
060928	<u>08 30 30.53</u>	<u>-42 45 01.8</u>	10.2 <sup>b</sup>	050724 <sub>71</sub>	<u>16 24 44.32</u>	<u>-27 32 26.4</u>	5.0 <sup>b</sup>
061025	<u>20 03 37.18</u>	<u>-48 14 28.9</u>	3.4 <sup>b</sup>	050726	13 20 12.16	-32 03 51.0	3.7 <sup>b</sup>
041223	06 40 47.39	-37 04 22.6	6.4 <sup>b</sup>	050730 <sub>28</sub>	14 08 17.12	-03 46 16.3	1.4 <sup>b</sup>
050117	<u>23 53 47.24</u>	<u>+65 56 00.2</u>	14.1 <sup>b</sup>	050801 <sub>72</sub>	13 36 35.51	-21 55 42.7	5.0 <sup>b</sup>
050124	12 51 30.43	+13 02 40.6	2.8 <sup>b</sup>	050802 <sub>33</sub>	14 37 05.91	+27 47 11.3	1.5 <sup>a</sup>
050126	18 32 27.22	+42 22 14.2	3.3 <sup>b</sup>	050803	23 22 37.87	+05 47 09.8	1.8 <sup>b</sup>
050128	14 38 17.66	-34 45 54.7	2.7 <sup>b</sup>	050813	<u>16 07 57.19</u>	<u>+11 14 57.8</u>	3.8 <sup>a</sup>
050215B <sub>44</sub>	11 37 47.74	+40 47 44.6	1.9 <sup>a</sup>	050814 <sub>10</sub>	17 36 45.31	+46 20 21.6	1.0 <sup>b</sup>
050219A	11 05 39.13	-40 41 02.6	3.5 <sup>b</sup>	050815 <sub>76</sub>	<u>19 34 22.80</u>	<u>+09 08 47.5</u>	7.9 <sup>b</sup>
050219B	05 25 15.76	-57 45 28.2	4.3 <sup>b</sup>	050819	<u>23 55 01.49</u>	<u>+24 51 39.9</u>	3.3 <sup>b</sup>
050223	18 05 32.66	-62 28 20.4	3.2 <sup>b</sup>	050820A <sub>6</sub>	22 29 38.08	+19 33 36.4	0.9 <sup>b</sup>
050306	18 49 14.43	-09 09 09.9	4.7 <sup>b</sup>	050820B	09 02 25.37	-72 38 43.7	5.2 <sup>b</sup>
050315 <sub>24</sub>	20 25 54.21	-42 36 02.5	1.4 <sup>b</sup>	050822	03 24 27.22	-46 02 00.0	0.7 <sup>b</sup>
050318 <sub>58</sub>	03 18 51.04	-46 23 43.5	2.7 <sup>b</sup>	050824	00 48 56.16	+22 36 33.4	1.0 <sup>b</sup>
050319 <sub>13</sub>	10 16 47.89	+43 32 53.3	1.1 <sup>a</sup>	050826 <sub>55</sub>	05 51 01.69	-02 38 37.6	2.6 <sup>b</sup>
050326	00 27 49.11	-71 22 16.4	2.9 <sup>b</sup>	050827	04 17 09.58	+18 12 00.4	1.3 <sup>b</sup>
050401 <sub>41</sub>	16 31 28.84	+02 11 14.5	1.8 <sup>b</sup>	050904	<u>00 54 50.93</u>	<u>+14 05 11.8</u>	1.2 <sup>a</sup>
050406 <sub>19</sub>	02 17 52.25	-50 11 15.0	1.3 <sup>b</sup>	050906	03 31 15.28	-14 36 30.1	15.7 <sup>b</sup>
050410	<u>05 59 13.94</u>	<u>+79 36 11.7</u>	2.3 <sup>b</sup>	050908 <sub>49</sub>	01 21 50.85	-12 57 17.9	2.2 <sup>b</sup>
050412 <sub>73</sub>	12 04 25.18	-01 12 00.8	6.9 <sup>a</sup>	050911	00 54 38.29	-38 50 58.5	2.1 <sup>b</sup>
050416A <sub>2</sub>	12 33 54.57	+21 03 26.9	0.6 <sup>a</sup>	050915A <sub>26</sub>	05 26 44.86	-28 00 59.9	1.4 <sup>b</sup>
050416B	08 55 34.91	+11 10 30.7	1.8 <sup>b</sup>	050915B	14 36 26.24	-67 24 31.7	4.1 <sup>b</sup>
050421	20 29 03.22	+73 39 18.9	3.3 <sup>b</sup>	050916	09 03 57.07	-51 25 43.4	5.7 <sup>b</sup>
050422	21 37 54.65	+55 46 46.4	1.5 <sup>b</sup>	050922B	00 23 13.19	-05 36 15.6	2.7 <sup>b</sup>
050502B	09 30 10.06	+16 59 46.5	1.0 <sup>a</sup>	050922C <sub>46</sub>	21 09 33.12	-08 45 28.3	2.0 <sup>b</sup>

Notes: Positions lying outside the refined XRT-Team error regions are underlined. <sup>a</sup>- Position matching with SDSS DR-5 catalog. <sup>b</sup>- with DSS-red2 catalog. The subscripts on some GRB names refer to Figure 3 and denote the bursts with OT positions. The first 17 bursts above were discovered by satellites other than Swift.

Table 2: Astrometrically-corrected XRT GRB Afterglow Positions (continued)

GRB	$\alpha$ (J2000)	$\delta$ (J2000)	Err <sub>90</sub> ["]	GRB	$\alpha$ (J2000)	$\delta$ (J2000)	Err <sub>90</sub> ["]
050925	20 13 47.57	+34 19 51.4	2.7 <sup>b</sup>	060322	18 16 56.54	-36 42 32.4	6.7 <sup>b</sup>
051001	23 23 48.73	-31 31 23.3	1.5 <sup>b</sup>	060323	11 37 45.19	+49 59 06.4	2.0 <sup>a</sup>
051006	07 23 14.03	+09 30 21.9	4.3 <sup>b</sup>	060403	18 49 21.44	+08 19 44.6	3.1 <sup>b</sup>
051008	13 31 29.55	+42 05 53.3	1.2 <sup>a</sup>	060413	<u>19 25 07.91</u>	<u>+13 45 30.1</u>	1.9 <sup>b</sup>
051016A	08 11 16.77	-18 17 53.7	2.2 <sup>b</sup>	060418 <sub>70</sub>	15 45 42.47	-03 38 20.1	4.9 <sup>b</sup>
051016B <sub>8</sub>	08 48 27.80	+13 39 20.7	0.9 <sup>a</sup>	060421	22 54 32.87	+62 43 50.1	1.6 <sup>b</sup>
051021B	08 24 11.98	-45 32 28.2	3.4 <sup>b</sup>	060427	08 17 04.53	+62 40 19.5	7.2 <sup>b</sup>
051109A <sub>15</sub>	22 01 15.32	+40 49 21.6	1.1 <sup>b</sup>	060428A	08 14 10.88	-37 10 11.2	0.8 <sup>b</sup>
051109B	23 01 50.32	+38 40 47.3	1.6 <sup>b</sup>	060428B <sub>27</sub>	15 41 25.72	+62 01 29.6	1.4 <sup>a</sup>
051111	23 12 33.22	+18 22 28.5	2.6 <sup>b</sup>	060501	<u>21 53 30.46</u>	<u>+43 59 54.8</u>	8.8 <sup>b</sup>
051117A <sub>31</sub>	<u>15 13 34.00</u>	<u>+30 52 10.9</u>	1.5 <sup>a</sup>	060502A <sub>45</sub>	<u>16 03 42.56</u>	<u>+66 36 02.9</u>	2.0 <sup>b</sup>
051117B	05 40 43.21	-19 16 27.2	2.0 <sup>b</sup>	060502B <sub>68</sub>	18 35 45.53	+52 37 52.9	3.7 <sup>b</sup>
051210	22 00 41.26	-57 36 46.5	2.9 <sup>b</sup>	060505	<u>22 07 03.39</u>	<u>-27 48 53.0</u>	2.5 <sup>b</sup>
051221A <sub>9</sub>	21 54 48.69	+16 53 28.0	0.9 <sup>b</sup>	060507	<u>05 59 50.62</u>	<u>+75 14 57.2</u>	1.4 <sup>b</sup>
051221B	20 49 35.10	+53 02 12.9	6.9 <sup>b</sup>	060510A <sub>42</sub>	06 23 27.90	-01 09 45.5	1.9 <sup>b</sup>
051227 <sub>57</sub>	<u>08 20 58.06</u>	<u>+31 55 34.2</u>	2.7 <sup>a</sup>	060510B	15 56 30.07	+78 34 12.4	2.9 <sup>b</sup>
060105	19 50 00.69	+46 20 55.9	1.3 <sup>b</sup>	060512 <sub>50</sub>	13 03 05.73	+41 11 26.9	2.4 <sup>a</sup>
060108 <sub>21</sub>	<u>09 48 02.00</u>	<u>+31 55 08.0</u>	1.3 <sup>a</sup>	060515	08 29 09.49	+73 34 00.3	4.7 <sup>b</sup>
060109	18 50 43.55	+31 59 28.3	1.8 <sup>b</sup>	060522 <sub>62</sub>	<u>21 31 45.02</u>	<u>+02 53 13.0</u>	2.8 <sup>b</sup>
060110 <sub>63</sub>	04 50 57.76	+28 25 55.0	2.9 <sup>b</sup>	060526 <sub>34</sub>	15 31 18.23	+00 17 05.4	1.6 <sup>a</sup>
060111A	18 24 49.20	+37 36 14.1	1.1 <sup>b</sup>	060602A	09 58 16.93	+00 18 12.8	2.3 <sup>b</sup>
060111B <sub>54</sub>	<u>19 05 42.75</u>	<u>+70 22 33.3</u>	2.6 <sup>b</sup>	060602B	<u>17 49 31.94</u>	<u>-28 08 05.8</u>	3.3 <sup>b</sup>
060115	<u>03 36 08.18</u>	<u>+17 20 44.3</u>	2.6 <sup>b</sup>	060604 <sub>11</sub>	<u>22 28 55.01</u>	<u>-10 54 55.9</u>	1.0 <sup>b</sup>
060116 <sub>64</sub>	05 38 46.14	-05 26 15.2	3.1 <sup>b</sup>	060605 <sub>60</sub>	21 28 37.30	-06 03 32.2	2.8 <sup>b</sup>
060124	05 08 26.00	+69 44 27.2	0.7 <sup>b</sup>	060607A <sub>37</sub>	<u>21 58 50.44</u>	<u>-22 29 48.1</u>	1.7 <sup>b</sup>
060202	02 23 23.01	+38 23 03.2	1.1 <sup>b</sup>	060614 <sub>23</sub>	21 23 32.04	-53 01 37.0	1.4 <sup>b</sup>
060203 <sub>14</sub>	06 54 04.05	+71 48 39.3	1.1 <sup>b</sup>	060707 <sub>36</sub>	23 48 19.07	-17 54 18.9	1.6 <sup>b</sup>
060204B	<u>14 07 15.05</u>	<u>+27 40 36.9</u>	1.6 <sup>a</sup>	060708 <sub>25</sub>	00 31 13.79	-33 45 33.3	1.4 <sup>b</sup>
060206 <sub>3</sub>	13 31 43.51	+35 03 02.8	0.8 <sup>a</sup>	060712	12 16 16.12	+35 32 17.7	1.5 <sup>a</sup>
060210 <sub>5</sub>	03 50 57.35	+27 01 34.3	0.9 <sup>b</sup>	060714 <sub>39</sub>	15 11 26.43	-06 33 59.5	1.8 <sup>b</sup>
060211A	03 53 32.63	+21 29 19.4	2.0 <sup>b</sup>	060717	11 23 21.74	+28 57 04.9	4.3 <sup>a</sup>
060211B	05 00 17.12	+14 56 58.1	1.9 <sup>b</sup>	060719 <sub>30</sub>	<u>01 13 43.69</u>	<u>-48 22 51.0</u>	1.5 <sup>b</sup>
060218 <sub>18</sub>	03 21 39.66	+16 52 02.1	1.2 <sup>b</sup>	060729 <sub>1</sub>	<u>06 21 31.90</u>	<u>-62 22 12.6</u>	0.5 <sup>b</sup>
060219	<u>16 07 21.54</u>	<u>+32 18 57.3</u>	1.6 <sup>a</sup>	060801	<u>14 12 01.35</u>	<u>+16 58 53.7</u>	2.4 <sup>a</sup>
060223A <sub>66</sub>	03 40 49.82	-17 07 49.8	3.4 <sup>b</sup>	060804 <sub>77</sub>	<u>07 28 49.60</u>	<u>-27 12 52.8</u>	10.8 <sup>b</sup>
060223B	<u>16 56 58.67</u>	<u>-30 48 35.4</u>	12.4 <sup>b</sup>	060805A	14 43 43.46	+12 35 11.8	1.8 <sup>a</sup>
060306	02 44 22.91	-02 08 54.0	1.3 <sup>b</sup>	060807 <sub>17</sub>	<u>16 50 02.58</u>	<u>+31 35 30.4</u>	1.2 <sup>a</sup>
060312	03 03 05.92	+12 50 02.0	2.0 <sup>b</sup>	060813	<u>07 27 35.23</u>	<u>-29 50 50.3</u>	2.2 <sup>b</sup>
060313 <sub>52</sub>	04 26 28.41	-10 50 40.7	2.4 <sup>b</sup>	060814	14 45 21.29	+20 35 10.7	0.9 <sup>a</sup>
060319	<u>11 45 32.89</u>	<u>+60 00 39.1</u>	0.9 <sup>b</sup>	060825	<u>01 12 29.46</u>	<u>+55 47 51.4</u>	2.9 <sup>b</sup>

Notes: Positions lying outside the refined XRT-Team error regions are underlined. <sup>a</sup>- Position matching with SDSS DR-5 catalog. <sup>b</sup>- with DSS-red2 catalog. The subscripts on some GRB names refer to Figure 3 and denote the bursts with OT positions.

Table 3: Astrometrically-corrected XRT GRB Afterglow Positions (continued)

GRB	$\alpha$ (J2000)	$\delta$ (J2000)	Err <sub>90</sub> ["]	GRB	$\alpha$ (J2000)	$\delta$ (J2000)	Err <sub>90</sub> ["]
060904A	15 50 54.56	+44 59 10.5	1.4 <sup>b</sup>	060927	21 58 12.23	+05 21 52.2	3.8 <sup>b</sup>
060904B <sub>38</sub>	<u>03 52 50.45</u>	<u>-00 43 30.0</u>	1.7 <sup>a</sup>	060929	17 32 28.98	+29 50 07.7	2.2 <sup>b</sup>
060906 <sub>53</sub>	<u>02 43 00.72</u>	<u>+30 21 43.2</u>	2.5 <sup>b</sup>	061002	14 41 23.40	+48 44 28.9	2.2 <sup>b</sup>
060908 <sub>56</sub>	<u>02 07 18.42</u>	<u>+00 20 30.8</u>	2.6 <sup>b</sup>	061004	06 31 10.93	-45 54 23.8	1.6 <sup>b</sup>
060912A <sub>43</sub>	00 21 08.11	+20 58 18.9	1.9 <sup>b</sup>	061006 <sub>51</sub>	07 24 07.56	-79 11 56.6	2.4 <sup>b</sup>
060919	18 27 41.89	-51 00 51.1	2.6 <sup>b</sup>	061007 <sub>32</sub>	03 05 19.55	-50 30 01.8	1.5 <sup>b</sup>
060923A <sub>65</sub>	16 58 28.05	+12 21 39.5	3.4 <sup>b</sup>	061019 <sub>74</sub>	06 06 30.80	+29 34 11.0	6.9 <sup>b</sup>
060923B	15 52 46.74	-30 54 11.3	7.4 <sup>b</sup>	061021 <sub>20</sub>	09 40 36.04	-21 57 04.9	1.3 <sup>b</sup>
060923C <sub>40</sub>	23 04 28.36	+03 55 28.4	1.8 <sup>b</sup>	061028	06 28 54.61	+46 17 57.5	2.7 <sup>b</sup>
060926 <sub>69</sub>	17 35 43.86	+13 02 19.0	4.6 <sup>b</sup>				

Notes: Positions lying outside the refined XRT-Team error regions are underlined. <sup>a</sup>- Position matching with SDSS DR-5 catalog. <sup>b</sup>- with DSS-red2 catalog. The subscripts on some GRB names refer to Figure 3 and denote the bursts with OT positions.

